



The CALIF 3 S-P 2 REMICS software: simulation of accelerated deflagrations using RANS and LES approaches

Bassam Gamal, Laura Gastaldo, Denis Veynante

► To cite this version:

Bassam Gamal, Laura Gastaldo, Denis Veynante. The CALIF 3 S-P 2 REMICS software: simulation of accelerated deflagrations using RANS and LES approaches. 10th European Combustion Meeting (2021), Apr 2021, Napoli (virtual conference), Italy. pp.1201-1206. <hal-03407108>

HAL Id: hal-03407108

<https://hal.science/hal-03407108v1>

Submitted on 28 Oct 2021

HAL is a multi-disciplinary open access archive for the deposit and dissemination of scientific research documents, whether they are published or not. The documents may come from teaching and research institutions in France or abroad, or from public or private research centers.

L'archive ouverte pluridisciplinaire **HAL**, est destinée au dépôt et à la diffusion de documents scientifiques de niveau recherche, publiés ou non, émanant des établissements d'enseignement et de recherche français ou étrangers, des laboratoires publics ou privés.



HAL Authorization

10TH
EUROPEAN
COMBUSTION
MEETING

April 14-15, 2021

Virtual Edition



PROCEEDINGS VOLUME

www.ecm2021napoli.eu

The CALIF³S-P²REMICS software: simulation of accelerated deflagrations using RANS and LES approaches

B. Gamal^{1,2,*}, L. Gastaldo¹, D. Veynante²

¹Institut de Radioprotection et de Sûreté Nucléaire (IRSN), Saint Paul Lez Durance, 13115, France

²Laboratoire EM2C, CentraleSupélec, Université Paris-Saclay, 3 rue Joliot Curie, 91190 Gif-sur-Yvette, France

Abstract

An accelerated deflagration in an obstructed rectangular semi-confined chamber has been simulated with three different configurations for the obstacles position. The simulations are performed with the in-house CALIF³S- P²REMICS software developed at IRSN. Two approaches have been considered. The first is based on a statistic description of the turbulence and on a turbulent flame-speed closure approach for combustion. The second one uses a LES approach for turbulence description. The combustion is modelled using a virtually thickened flame formalism (TFLES) combined with a dynamical determination of the sub-grid scale flame wrinkling factors to handle unresolved contributions.

1. Introduction

Accelerated turbulent deflagrations, potentially transiting to detonation, are a major hazard in industrial plants, and more specifically in nuclear power plants. The French Institut de Radioprotection et de Sûreté Nucléaire (IRSN) aims to enhance its capability of predictive risk evaluation in this field. Thus, IRSN is developing a simulation tool, named P²REMICS (for Partially PREMIXed Combustion Solver), to compute the formation of explosive atmospheres, their deflagration or detonation and the subsequent propagation of blast waves. The P²REMICS [1] software is built as a specific application of the generic CFD solver library CALIF³S [2] (for Components Adaptive Library For Fluid Flow Simulations), which deals with a wide range of applications, including laminar and turbulent flows, potentially reactive, governed by incompressible, low Mach number or compressible Navier-Stokes equations. Both P²REMICS and CALIF³S are in-house IRSN softwares, released under an open-source license.

To describe turbulence, a wide range of RANS models are available (high-Reynolds variants, with usual wall laws, and low-Reynolds models), together with Large Eddy Simulation models. Two different but complementary approaches are available for the turbulent deflagration modelling. The first one is based on RANS description of turbulence and on a *turbulent flame-speed closure* combustion model. The second one, based on an LES approach, uses a virtually thickened flame formalism (TFLES) combined with a dynamical determination of the sub-grid scale flame wrinkling factors to handle unresolved contributions.

In this paper, an accelerated deflagration test case is investigated. Simulations are performed with both, large eddy simulation and RANS approaches. The influence of the obstacles locations on the flame propagation is studied.

The paper is structured as follows. After a detailed description of both RANS and LES approaches for the simulation of accelerated deflagrations (Section 2), the experimental set up is presented (Section 3). Then, the numerical results obtained are detailed (Section 4).

2. Combustion modeling

2.1. Reynolds-averaged Navier-Stokes approach

For the simulation of turbulent deflagrations, a *turbulent flame-speed closure model* is implemented in P²REMICS. The flame brush location is determined by a phase-field-like technique, solving a transport equation for a characteristic function (more precisely speaking, a *Hamilton-Jacobi* equation), leading to a formulation which is reminiscent of the so-called *G*-equation based models [18]. The unknown of this transport equation is thus denoted here by *G* and referred to hereafter as the "*G*-field". Flame ignition is obtained by setting *G* = 0 in a small neighbourhood of the ignition point and *G* = 1 elsewhere. The classical reactive formulation of the chemical species mass balance equations is kept to cope with partially premixed situations. The reaction term is evaluated as a function of *G*: it is set to zero in the fresh zone (*G* ≥ 0.5), and to a finite (but possibly large) value in the burnt zone (*G* < 0.5). A one-step irreversible total chemical reaction is considered, the rate of progress of the reaction is supposed to vanish when either the fuel mass fraction *y_F* or the oxidant mass fraction *y_O* vanish and, as announced, is governed by the value of *G* [1, 16]:

$$\dot{\omega} = \frac{v_f}{\delta} \eta(y_F, y_O) (G-0.5)^-, \quad \eta(y_F, y_O) = \min\left(\frac{y_F}{v_F W_F}, \frac{y_O}{v_O W_O}\right)$$

where for $a \in \mathbb{R}$, $a^- = -\min(a, 0)$, v_f is the turbulent flame velocity, v_F and v_O are the fuel and oxidant molar stoichiometric coefficients, W_F and W_O stand for the molar masses of the fuel and oxydant respectively. δ is a quantity homogeneous to a length scale, which governs the thickness of the reaction zone.

The so-called *k* – ω model (with *k* the kinetic energy associated to velocity fluctuations) is used to describe turbulence [19].

The model is closed by a correlation for the turbulent flame speed. The correlation developed by Goulier *et al* [17] is retained here and reads:

$$v_f = \max(s_l, s_l 1.613 \left(\frac{r}{l_t}\right)^{0.333} \left(\frac{u'}{s_l}\right)^{0.526} \text{Le}^{-0.14}),$$

where u' is the root mean square of the velocity fluctuations, l_t is the integral length scale of turbulent structures, s_l is the laminar flame speed, r stands for the distance between the flame front and the ignition point and Le is the Lewis number of the unburnt mixture.

*Corresponding author: bassam.gamal@irsn.fr



2.2. Large eddy simulation approach

The experimental characterization of the velocity field during a deflagration is difficult, especially in medium and large-scale configurations. Moreover, turbulent flame speed correlations in literature assume an equilibrium between turbulence motions and flame surface wrinkling, generally not verified in unsteady flames, and display a large scatter. Finally, at early stages of the transient, the flame is laminar and propagates in a flow essentially at rest. Then, the flame is progressively wrinkled by turbulent motions generated by thermal expansion around obstacles and accelerates. Thus, the model used should be able to reproduce the laminar to turbulent transition. RANS models, mainly developed under homogeneous isotropic turbulence assumptions, generally fail in these situations. For these reasons, a large eddy simulation (LES) approach is developed.

The combustion is modelled using a virtually thickened flame formalism (TFLES). The flame front is artificially thickened by multiplying species and heat diffusion by a thickening factor \mathcal{F} and dividing the reaction rates by the same factor [4]. The modified flame front of thickness $\mathcal{F}\delta_L^0$ propagates at the same laminar flame speed s_l as the original flame. At the subgrid scale, the thickened front is less sensitive to turbulence due to the diminution of the Damkohler number [9]. A wrinkling factor Ξ_Δ is introduced to model the subgrid scale flame surface, Δ being the combustion filter. The turbulent flame speed propagates at $s_T = \Xi_\Delta s_l$ [10].

Various models have been developed for the wrinkling factor. Algebraic expressions assume an equilibrium between turbulence and flame surfaces and often involve quantities such as the sub-grid scale turbulence intensity requiring modeling [11]. The sub-grid scale wrinkling factor Ξ_Δ is written here:

$$\Xi_\Delta = \left(\frac{\Delta}{\delta_c} \right)^\beta \quad (1)$$

where β is the model parameter and δ_c is the inner cutoff scale (*i.e.* the lowest wrinkling scale) identified here to the laminar flame thickness.

The model parameter β is dynamically determined [13, 8] equating flame surfaces computed at filtered and test-filtered scales (Germano-like identity) [12]:

$$\langle \Xi_\Delta |\widehat{\nabla \tilde{c}}| \rangle = \langle \Xi_{\gamma\Delta} |\nabla \hat{c}| \rangle \quad (2)$$

where c stands for the progress variable, increasing from 0 in fresh to 1 in burnt gases and computed here from the fuel mass fraction. The $\hat{\cdot}$ symbol denotes the Gaussian test-filtering operator and $\langle \cdot \rangle$ denotes the averaging operator over the entire domain. The effective filter scale is given by $\gamma = \sqrt{1 + (\hat{\Delta}/\Delta)^2}$ when combining two Gaussian filters of width $\hat{\Delta}$ and Δ [15]. The model parameter β is given by combining equations (1) and (2) and assuming that β is equal at scales $\hat{\Delta}$ and $\gamma\Delta$ and constant over the averaging domain:

$$\beta = \frac{\log(|\widehat{\nabla \tilde{c}}|/|\nabla \hat{c}|)}{\log(\gamma)} \quad (3)$$

Unphysical wrinkling factors values greater than unity may appear when the flame front interact with walls, the subgrid model is slightly modified near walls by replacing $|\nabla \hat{c}|$ in

(3) by $|\widehat{\nabla \tilde{c}}|$ [14]. Moreover, when more than one flame front interact at scale $\hat{\Delta}$, the wrinkling factor definition is no more valid as $|\nabla \hat{c}|$ may tend to zero. To overcome this difficulty, a sensor denoted by ζ is introduced in order to detect flame front interactions and defined as:

$$\zeta = \begin{cases} 1 & \text{if } \mathbf{n} \cdot \mathbf{N} < 1 - \varepsilon \\ 0 & \text{elsewhere} \end{cases}$$

where $\mathbf{n} = -\nabla \tilde{c}/|\nabla \tilde{c}|$ and $\mathbf{N} = -\nabla \hat{c}/|\nabla \hat{c}|$ and the parameter ε is set in the simulations showed in this paper to 0.1. The subgrid model is then corrected by replacing $|\nabla \hat{c}|$ in (3) by [14]:

$$(1 - \zeta)|\nabla \hat{c}| + \zeta|\widehat{\nabla \tilde{c}}|\mathbf{n} \cdot \mathbf{N}$$

The reaction rate is calculated with the Arrhenius law assuming a single step chemical reaction [5]. The activation energy and the pre-exponential factor are set as $E_a = 8.36 \times 10^4 \text{ J.mol}^{-1}$ and $A = 3.402 \times 10^7 \text{ uSI}$.

3. Experimental set up

The experimental configuration investigated by Wen *et al* [3] is retained for numerical simulations. The combustion chamber has a 150 mm square cross section and a height of 500 mm. The bottom of the chamber is fully closed whereas the top is an open end, sealed with a thin polyvinyl chloride membrane to contain the premixed flammable mixture. When deflagration occurs, the membrane is ruptured allowing unburned and burned mixtures to escape. The chamber is equipped by three obstacles of 75 mm in length, 150 mm in width and 10 mm in height, designated by S1, S2 and S3 in Figure 1. The first one is located at 100 mm from the bottom of the facility. The distance between the obstacles is 100 mm. Three configurations with different transverse obstacle locations are studied here (see Figure 1). For the first one, the obstacles are placed at the center of the chamber. In the second one, the obstacles are all on one side of the chamber and in the third configuration, obstacles are staggered on both sides of the chamber.

The explosive atmosphere is a stoichiometric methane-air mixture at initial ambient pressure and temperature. Initially the fluid is assumed to be at rest in the device. The ignition point is located at the bottom of the facility (see Figure 1). Overpressure is detected with a pressure transmitter at the bottom of the chamber next to the ignition location.

4. Numerical results

4.1. Numerical set up

The simulations are performed on a 2D computational domain. Outside the combustion chamber, the computational domain is extended in order to allow a more realistic reproduction of the exit of the expanding gas from the combustion chamber into the atmosphere and to avoid the reflexion on the boundary of the pressure waves generated by the deflagration. The computational domain is the same for both LES and RANS simulations. The mesh is composed by a non-uniform structured grid with rectangular cells. The space step in the chamber is uniform and set to 0.25 mm for LES simulations (respectively to 0.5 mm for RANS simulations). The total number of cells is close



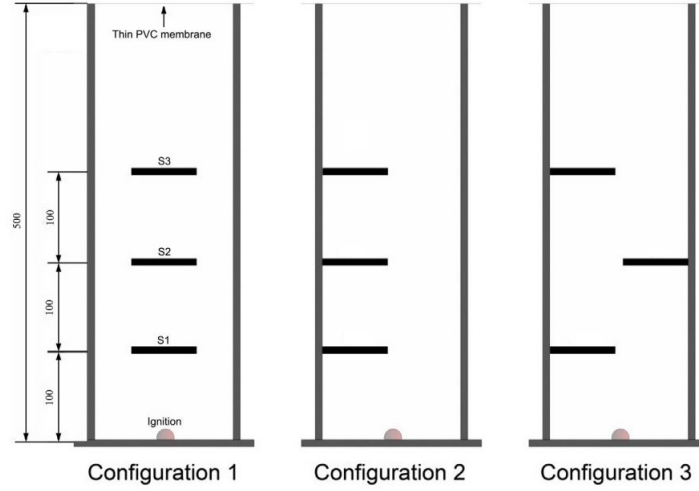


Figure 1: Experimental set up

to 1200000 for LES simulations (respectively 600000 for RANS simulations). Adiabatic and no-slip wall boundary conditions were applied at the solid interfaces (bottom and vertical faces of the chamber, faces of the obstacles). The time step is computed in order to have an acoustic Courant-Friedrichs-Lewy condition $CFL = 0.2$ for LES computations and a $CFL = 0.5$ for RANS computations. The three obstacles configurations have been studied with the LES approach, but only the third one has been simulated with the RANS modeling.

For LES computations, the thickening factor \mathcal{F} is calculated as a function of the laminar flame thickness δ_L^0 and the space step Δ_x such as $\mathcal{F} = n\Delta_x/\delta_L^0$, with $n = 15$ the number of cells needed to resolve the flame front. The wrinkling factor Ξ_Δ is computed dynamically every 150 time steps (corresponding approximatively to $9 \mu s$) in order to save computational cost linked to the filtering operation. The distance traveled by a convected fluid particle during $9 \mu s$ is lower than 0.35 mm which is acceptable regarding the filter size. The ignition is made with an initial flame kernel radius $r_c = 8 \text{ mm}$ by initializing the temperature and the fuel mass fraction with an expression such as:

$$\frac{1}{2} \left[1 + \operatorname{erf} \left(\frac{2}{\mathcal{F}\delta_L^0} (r - r_c) \right) \right] x_u \quad (4)$$

where x_u is the fuel mass fraction or the temperature in the fresh gases and r stands for the distance between the flame front and the ignition point. Such initialization has the advantage of avoiding any complex ignition scheme and directly set the flame front to a thickness $\mathcal{F}\delta_L^0$. A backward time shift for each simulation is applied to numerical results in order to match the overpressure peak. The main reasons of this delay is due to the lack of ignition model.

4.2. Flame front structure

The numerical flame shapes are compared to the experimental high-speed images of flame structures [3]. Here only the results obtained with the LES approach for configuration 3 are plotted in Figure 2. Figure 2a shows the temperature field with the velocity vectors.

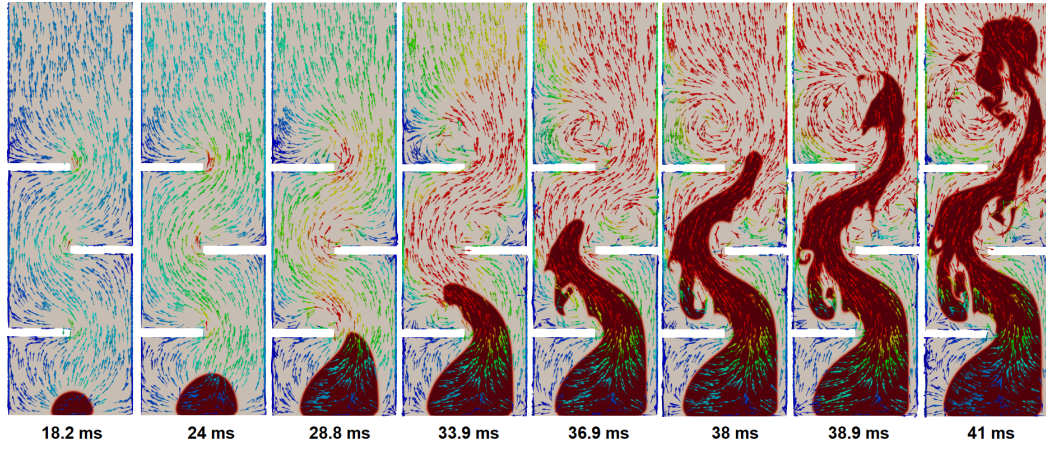
Initially the flame structure is similar for the three configurations (first frame of Figure 2). The flame is initially

laminar and propagates slowly with a spherical shape. Turbulence is generated downstream obstacles by the thermal expansion of burnt gases. Before the flame arrival to the first obstacle, the flame front structure differs from one configuration to the other. The front flattens off slightly for the first configuration. In both configurations 2 and 3, the flame fronts gradually distort and tend to move toward the opposite side of the facility (second frame of Figure 2). In the experiment, the time needed for the flame to reach the first obstacle is about 27 ms , which is less than for configuration 1 (30 ms). At this stage, the numerical flame shape is close to the experimental one for both LES and RANS approaches but the simulated flame front reaches the first obstacle later than the experiment. This inaccuracy in the flame velocity in the early stages of the experiment is not surprising. Indeed, no ignition model is used for both LES and RANS approaches. Moreover, the RANS model is designed for situations where the turbulence is fully developed, which is not the case at the beginning of the transient.

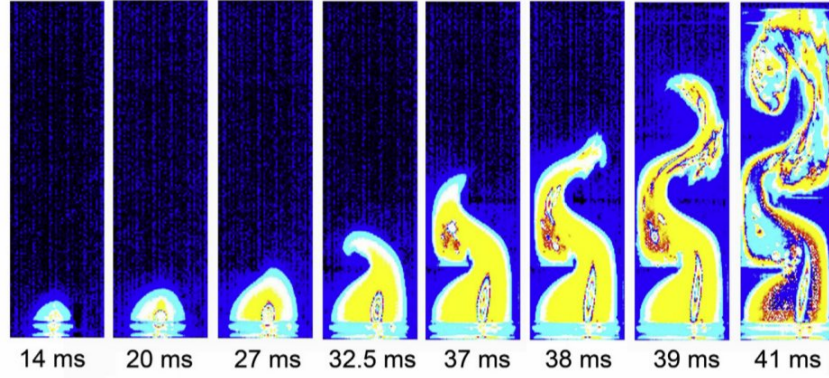
The flame accelerates due to obstructions, but the flame is faster in configurations 1 and 3 with respect to configuration 2. This is due to a higher level of turbulence intensity resulting from the flame obstacles interactions. As shown in Figure 2, the flame structures become distorted and turbulent and the flame surfaces increase. This is well reproduced by LES simulations, whereas the flame front obtained RANS simulations is smoother.

Experimentally, the flames exit the chamber faster in configuration 1 (40.5 ms), even though the flame propagates slowly in the initial stages [3]. This result is probably due to the fact that after passing the first obstacle, a pair of symmetrical flames develops, the flame surface is thus higher than those in the other two configurations and may lead to a more significant increase in burning rate and thus flame speed. The slower flame is obtained with the second configuration. The flame exits the chamber after 43.5 ms . LES results are in agreement with experimental data. The numerical flames exit the chamber in configuration 1 after 40.7 ms and after 44 ms in configuration 2. Regarding the third configuration, as shown in Figure 2, the experimental flame exits the chamber at 41 ms . Once again, LES allows a good representation of the eddies wrinkling the flame and





(a) LES snapshots of the temperature field and velocity vectors



(b) Sequential images

Figure 2: Snapshots (a) and experimental images (b) showing deflagration flame propagation in configuration 3 from Weng *et al.* [3]

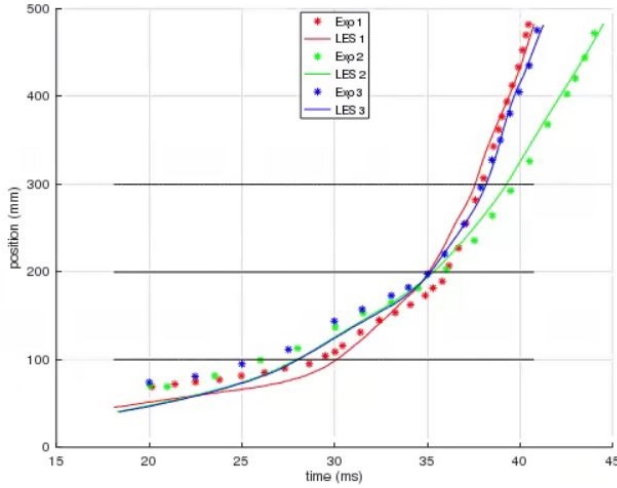


Figure 3: Flame position for all configurations

the same behavior is recovered. The flame exits the chamber after 41.5 ms (last snapshot of Figure 2). With RANS approach, the shape of the flame is thinner and the flame exits earlier at 38 ms.

4.3. Flame front position

In Figure 3 the flame front positions obtained with LES approach are compared to experimental data for all configurations [3]. The horizontal black lines corresponds to the location of the obstacles. The location is measured as the maximum axial distance of the flame front from the chamber bottom. Before the first obstacle, the flame position in-

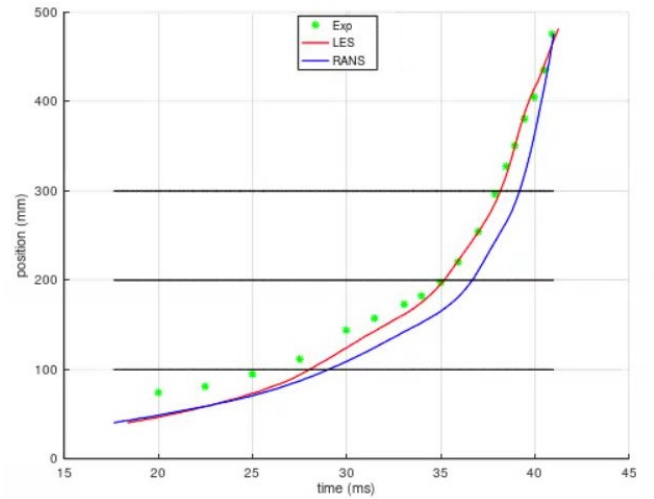


Figure 4: RANS and LES flame position for configuration 3

creases linearly through time matching the laminar flame speed. Then, flow vortices appear behind each obstacle, the flame become turbulent and the flame surface area increases. The flame continue to accelerate until reach the exit of the chamber. The second configuration flame front is slower than the first one, which can be explained by a weaker turbulence intensity. LES results match the experimental data. After comparasion with the non dynamical wrinkling factor, the dynamical formulation of the wrin-



klung factor turns out to be essential to catch the transition from laminar to turbulent regimes. For configuration 1, the numerical slope is steeper in the region between the first and the last obstacles. The flame is thus faster in this region with respect to experimental data.

In Figure 4, the flame front positions obtained with RANS and LES approaches are compared to experimental data for configuration 3 [3]. When the flame is laminar, RANS and LES computations are very similar in the early stage of the transient, even though RANS approach reaches the first obstacle a bit latter than the LES approach (28 ms for LES, 29 ms for RANS compared to 27 ms for the experimental value). After then, LES approach gives even more accurate results. Indeed at this stage, the flame is progressively wrinkled by turbulent motions generated by thermal expansion around obstacles and accelerates. Thus, the model used should be able to reproduce the laminar to turbulent transitions. RANS models, mainly developed under homogeneous isotropic turbulence assumptions, generally fail in these situations.

4.4. Overpressure dynamics

A particular interest is given to the overpressure prediction as the overpressure peak is representative of the damages resulting an explosion. In Figure 5, the predicted pressure time evolution for the configurations 1 and 2 are compared to the experimental data [3].

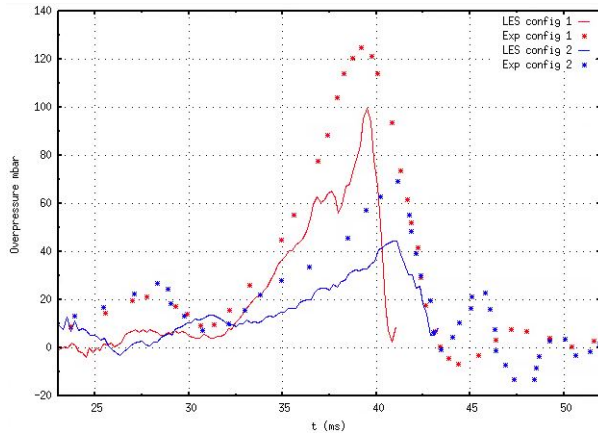


Figure 5: Experimental, RANS and LES flame overpressure

The experimental overpressures show two peaks for both configurations, the first ones correspond to the sealing film disintegration at the end of the chamber and is not recovered in the simulations. The second ones occur at 39 ms and 41.5 ms, for configurations 1 and 2 respectively. For configuration 1, the overpressure peak corresponds experimentally to the time when the flame front reconnects after crossing the last obstacle [3]. For configuration 2, it occurs experimentally when the flame front is located between the last obstacle and the chamber exit. LES results show that the second peak, for configurations 1 and 2, occur just before the time when the flame exits the open end. This is probably due to the fact that the flame fronts reconnect further in the facility. Configuration 2, produces the lowest peak overpressure of 69 mbar, whereas configuration 1 produces a peak overpressure of 124 mbar. Numerically, the peak of pressures are underestimated for both first and second configurations (the maximum overpressures are around

15 mbar lower than the experiment values). Small fluctuations are observed in LES. These fluctuations are due to the reflexion of the pressure waves relexions on the walls.

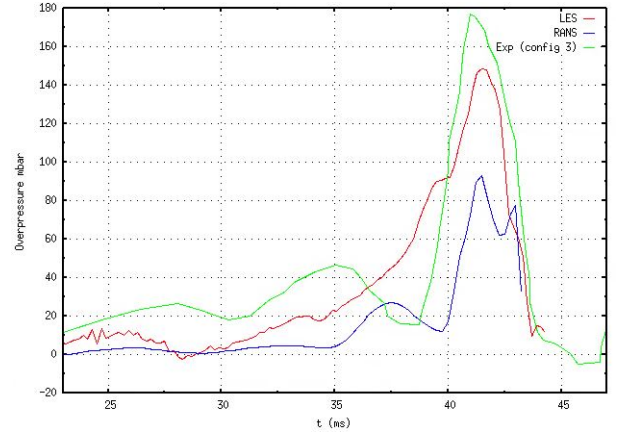


Figure 6: Experimental, RANS and LES flame overpressure

In Figure 6, the computed pressure evolution with the RANS and LES modeling for the configuration 3 are compared to the experimental data [3]. The overpressure evolution is similar to those reported for configurations 1 and 2. Moreover the overpressure reached is higher than those of configurations 1 and 2 (183 mbar). This may be due to the more significantly turbulent flow condition induced by the staggered obstacles. The peak obtained by LES and RANS configurations is obtained at 41 ms, as in the experiment, just before the flame exits (last snapshot of Figure 2 for LES approach). But the pressure is underestimated by both approaches, mostly by the RANS one.

4.5. Flame surface

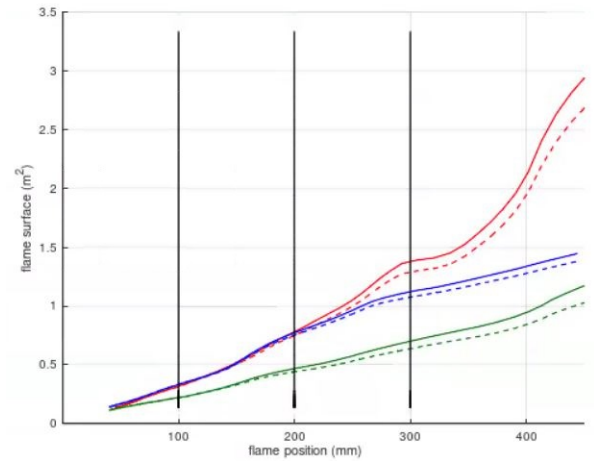


Figure 7: Flame surface and total flame surface with LES for the three configurations

For LES, a way to observe the effect of the subgrid scale model is to plot the resolved flame surface $S_r(t)$ and the total flame surface $S_t(t)$ [7] which are defined as follows:

$$S_r(t) = \int_{\mathcal{V}} |\nabla \tilde{c}| d\mathcal{V}, \quad S_t(t) = \int_{\mathcal{V}} \Xi_{\Delta} |\nabla \tilde{c}| d\mathcal{V} \quad (5)$$

The resolved and total flame surfaces for the three configurations are reported in Figure 7, the dashed lines are the resolved flame surfaces and the solid lines are the total flame surfaces. The red color corresponds to configuration

1, blue to configuration 2 and green to configuration 3. Before the flame front reaches the first obstacle, the flame front is not wrinkled yet by turbulence, thus $\Xi_{\Delta} = 1$, total and resolved flame surface curves match. Afterwards, turbulence wrinkles the flame front and the efficiency factor increases leading to a higher value of the total flame surface. Yet, the difference between the total flame surface and the resolved flame surface stays relatively small even if the experiment is quite turbulent. This shows that the major part of the flame surface is resolved in the simulation.

5. Conclusion

A deflagration accelerated by obstructions in an open chamber has been simulated with the in-house software CALIF³S- P²REMICS. Two different approaches have been used for the turbulent deflagration modelling. In the first one, the turbulence is modelled by a Reynolds-averaged Navier-Stokes (RANS) approach and the combustion model relies on a *turbulent flame-speed closure*. In the second one, a large eddy simulation (LES) approach is used for turbulence. The combustion is modelled using a virtually thickened flame formalism (TFLES) combined with a dynamical determination of the sub-grid scale flame wrinkling factors to handle unresolved contributions. The influence of the location of obstacles on the flame propagation has been studied. Generally speaking, numerical results are in reasonable agreement with the experimental ones for both approaches. However, LES results highlight the importance of the wrinkling factor dynamical formulation to catch the transition from laminar to turbulent regimes. The RANS approach, mainly developed under homogeneous isotropic turbulence assumptions, fail in this situation.

6. References

- [1] P²REMICS Collaborative website, Physical Modelling in P²REMICS, IRSN, <http://gforge.irsnn.fr/gf/project/p2remics>.
- [2] CALIF³S. Collaborative development environment, IRSN, <https://gforge.irsnn.fr/gf/project/calif3s>.
- [3] X. Wen, M. Yu, Z. Liu, G. Li, W. Ji, M. Xie, Effects of cross-wise obstacle position on methane air deflagration characteristics, *Journal of Loss Prevention in the Process Industries*, 26, (2013), pp. 1335-1340.
- [4] T. Butler, P. O'Rourke. A numerical method for two dimensional unsteady reacting flows, *Symp. (Int.) Combustion.*, 16, (1977), pp. 1503-1515.
- [5] T. Poinso, D. Veynante. Theoretical and numerical combustion, (2011), 3rd edition, <http://elearning.cerfacs.fr/combustion/onlinePoinso-Book/buythirdedition/index.php>.
- [6] P. Volpiani, T. Schmitt, O. Vermorel, P. Quillatre, D. Veynante, Large eddy simulation of explosion deflagrating flames using a dynamic wrinkling formulation, *Combustion and Flame*, Volume 186, (2017), pp. 17-31.
- [7] P. Volpiani, T. Schmitt, D. Veynante, A posteriori tests of a dynamic thickened flame model for large eddy simulations of turbulent premixed combustion, *Combustion and Flame*, Volume 174, (2016), pp. 166-178.
- [8] D. Veynante, V. Moureau, Analysis of dynamic models for large eddy simulations of turbulent premixed combustion, *Combustion and Flame*, Volume 162, (2015), pp. 4622-4642.
- [9] O. Colin, F. Ducros, D. Veynante, T. Poinso, A thickened flame model for large eddy simulation of turbulent premixed combustion, *Phys. Fluids*, 12, (2000), pp. 1843-1863.
- [10] F. Charlette, C. Meneveau, D. Veynante, A power-law flame wrinkling model for LES of premixed turbulent combustion part I: non-dynamic formulation and initial tests, *Combustion and Flame*, 131, (2002), pp. 159-180.
- [11] F. Charlette, C. Meneveau, D. Veynante, A power-law flame wrinkling model for LES of premixed turbulent combustion part II: non-dynamic formulation and initial tests, *Combustion and Flame*, 131, (2002), pp. 181-197.
- [12] M. Germano, U. Piomelli, P. Moin, W.H. Cabot, A dynamic subgrid-scale eddy viscosity model, *Phys. Fluids*, A 3, (1991), pp. 1760-1765.
- [13] T. Schmitt, M. Boileau, D. Veynante, Flame wrinkling factor dynamic modeling for large eddy simulations of turbulent premixed combustion, *Flow Turbul. Combust.*, 94, (2015), pp. 199-217.
- [14] S. Mouriaux, O. Colin, D. Veynante, Adaptation of a dynamic wrinkling model to an engine configuration, *Proc. Combust. Inst.*, (2016), pp. 159-180.
- [15] V. Moureau, P. Domingo, L. Vervisch, From large-eddy simulation to direct numerical simulation of a lean premixed swirl flame: filtered laminar flame-pdf modeling, *Combust. Flame* 158, (2011), pp. 1340-1357.
- [16] L. Gastaldo, F. Babik, F. Duval, C. Lapuerta, J.-C. Latché, Simulation of accelerated deflagration using the P²REMICS software, 17th Symposium NURETH, China, (2017).
- [17] J. Goulier, Comportements aux limites de flammes de prémélange hydrogène/air. tude de la transition flamme laminaire-flamme turbulente, PhD Thesis - Université d'Orléans, (2015).
- [18] A.N. Lipatnikov and J. Chomiak, Turbulent flame speed and thickness: phenomenology, evaluation, and application in multi-dimensional simulations, *Progress in Energy and Combustion Science*, 28, (2002), 1-74.
- [19] F. R. Menter, M. Kuntz and R. Langtry, Ten Years of Industrial Experience with the SST Turbulence Model, K. Hanjalic, Y. Nagano, and M. Tummers, Begell Housera, Inc., *Turbulence, Heat and Mass Transfer*, 4, (2003), 625-632.

